Atmos. Chem. Phys. Discuss., https://doi.org/10.5194/acp-2019-161
Manuscript under review for journal Atmos. Chem. Phys.
Discussion started: 18 March 2019
© Author(s) 2019. CC BY 4.0 License.

Atmospheric Chemistry and Physics Discussions

Soil emissions, soil air dynamics and model simulation of gaseous mercury in subtropical forest

Jun Zhou [a, b, c], Zhangwei Wang [a, b, *], Xiaoshan Zhang [a, b], Charles T. Driscoll [d], Che-Jen Lin [e]

a. Research Center for Eco-Environmental Sciences, Chinese Academy of Sciences, Beijing 100085, China

b. University of Chinese Academy of Sciences, Beijing 100049, China.

c. Key Laboratory of Soil Environment and Pollution Remediation, Institute of Soil Science, Chinese Academy of Sciences, Nanjing 210008, China

d. Department of Civil and Environmental Engineering, Syracuse University, 151 Link Hall, Syracuse, New York 13244, United States

e. Center for Advances in Water and Air Quality, Lamar University, Beaumont, Texas 77710, United States

* Corresponding author: Zhangwei Wang

E-mail address: wangzhw@rcees.ac.cn(Z. Wang); Phone: +86 10 62849168.

No.18 Shuangqing Road, Beijing 100085, China

First author e-mail: zhoujun@issas.ac.cn (J. Zhou).

Atmos. Chem. Phys. Discuss., https://doi.org/10.5194/acp-2019-161
Manuscript under review for journal Atmos. Chem. Phys.
Discussion started: 18 March 2019
© Author(s) 2019. CC BY 4.0 License.

Atmospheric Chemistry and Physics Discussions

Abstract: Evasion from soil is the largest source of mercury (Hg) to the atmosphere from terrestrial ecosystems. To reduce the uncertainty in estimates of Hg emissions from forest soils, soil-air total gaseous Hg (TGM) fluxes and vertical profiles of soil pore TGM concentrations were measured simultaneously for 130 days to improve parameterization of emission models. The soil-air TGM fluxes, measured using dynamic flux chambers (DFC), showed patterns of both emission and deposition at five study plots, with an area-weighted net emission rate of 3.2 ng m^{-2} hr^{-1}. The highest fluxes and net soil Hg emission were observed for an open field, with lesser emission rates in coniferous (pine) and broad-leaved (camphor) forests, and net deposition in a wetland. Fluxes showed strong positive relationships with solar radiation, soil temperature and soil Hg concentrations, and negative correlations with ambient-air TGM concentration and soil moisture. Using experimental field flux observations and quadratic relationships with the five parameters, four empirical models were developed to estimate soil-air TGM fluxes. The highest TGM concentrations in soil gas consistently occurred in the upper mineral horizons in the coniferous (pine) forest and in the organic horizon in the broad-leaved forest. Strong correlations between fluxes and TGM concentrations in upper soil horizons (0–10 cm) suggest that TGM in the pores of surface soil acts as the source for diffusion to the atmosphere. The TGM diffusion coefficients (D_s) between soil and atmosphere was firstly investigated at the field sites, with the range of 0.0042–0.013 m^2 hr^{-1}. These values should provide a foundation for future model development.

Keywords: soil-air flux; modeling; budget; soil profile of gaseous Hg; diffusion coefficient

Atmos. Chem. Phys. Discuss., https://doi.org/10.5194/acp-2019-161
Manuscript under review for journal Atmos. Chem. Phys.
Discussion started: 18 March 2019
© Author(s) 2019. CC BY 4.0 License.

Atmospheric Chemistry and Physics Discussions

1. Introduction

Global long-range atmospheric transport and deposition are the main pathway for mercury (Hg) input to remote ecosystems (Grigal, 2003;Obrist et al., 2018). Soils account for more than 90% of Hg stored in terrestrial ecosystems (Obrist, 2012;Zhou et al., 2017a). While most studies have focused on the Hg derived from anthropogenic emissions, recent global Hg models estimate that 3600 ± 3200 Mg yr^{-1} of atmospheric Hg is deposited to terrestrial surfaces, with 1000 ± 2000 Mg yr^{-1} re-emitted back to the atmosphere (Outridge et al., 2018). Additionally, compared to anthropogenic emissions of Hg (2500 Mg yr^{-1}), estimates of re-emissions from soil surfaces are highly uncertain (Agnan et al., 2016;Outridge et al., 2018;Wang et al., 2018). Compiling data from 132 studies, Agnan et al. (2016) suggest that the Earth's surface (particularly in East Asia) is an increasingly important source of total gaseous Hg (TGM) emissions, contributing up to half of the global emissions from natural sources. They estimated terrestrial TGM emissions of 607 Mg yr^{-1}, but with a large uncertainty range of −513 to 1353 Mg yr^{-1}.

Forest soils receive Hg inputs from the oxidation of atmospheric elemental Hg (Hg0) on foliage surfaces followed by wet deposition, leaching from throughfall, absorption of Hg^0 through plant stomata with litterfall inputs, or direct deposition from the atmosphere as dry deposition (Grigal, 2003;Teixeira et al., 2018;Risch et al., 2017), while Hg outputs from forests soil occur from surface or subsurface runoff and air-surface evasion. Forest soils are highly complex media, with important characteristics that affect air-soil exchange, including soil physio-chemical characteristics (e.g., porosity, oxygen availability, redox potential, organic matter, pH) (Moore and Castro, 2012;Obrist et al., 2010). Other factors also influence this process, such as meteorological conditions (e.g., solar radiation, air temperature, rainfall) (Eckley et al., 2015;Li et al., 2010;Zhou et al., 2015), atmospheric chemistry (ozone, nitrate radicals) (Peleg et al., 2015), atmospheric TGM concentrations (Wang et al., 2007) and biological processes (Obrist et al., 2010). Therefore, to characterize and quantify land-atmosphere exchange of TGM and eventually model global terrestrial sources to the atmosphere, it is necessary to understand how these factors mediate this process.

Research should not only focus on the magnitude of Hg emitted from soils and the environmental factors that influence the reduction of ionic Hg (Hg^{2+}) associated with the soil surfaces to Hg^0, but also the physical and chemical dynamics of Hg within soils is essential to fully

© Author(s) 2019. CC BY 4.0 License.

understand the regional and global atmospheric Hg budgets (Sigler and Lee, 2006). Numerous studies have researched soil-air Hg exchange by direct observations in the field or controlled experiments in the laboratory (Agnan et al., 2016;Zhu et al., 2016). A few studies have attempted to directly measure pore Hg concentrations within intact soils in the field (Moore and Castro, 2012;Obrist et al., 2017;Obrist et al., 2014;Sigler and Lee, 2006) and laboratory (Pannu et al., 2014) to quantify Hg^0 formation in soil pores. To date, only one study has examined TGM concentrations in soil pores and soil-air flux simultaneously. Unfortunately, those measurements were limited in temporal and spatial resolution (Sigler and Lee, 2006). The dynamics of gaseous Hg concentrations in soil profiles, the potential diffusive immobilization of pore Hg in soils, and the contribution of surface soils to the supply of atmospheric Hg are poorly understood and limit the development of models of land-atmosphere exchange of TGM.

In this paper, we present results of 130-day and multi-plot (five) study of soil-air fluxes and the vertical distribution of TGM in a subtropical forest located in Tieshanping Forest Park (TFP) in China conducted during different seasons in 2014. This study is, to our knowledge, the first direct field measurement of TGM diffusion coefficients between soil and the atmosphere. The aims were to (1) conduct field measurements to reduce the uncertainty in soil-air fluxes of TGM in forest catchments; (2) improve an empirical model of soil Hg evasion over complex terrain; and (3) understand how vertical profiles of TGM in soil pores evolve temporally and spatially and are related to soil-air exchange of Hg.

2. Materials and methods

2.1. Study area

The fluxes measurement were conducted in a Masson pine (*Pinus massoniana* Lamb.) stand (conifer), which was planted in 1960s following a complete destruction of a natural Masson pine forest at TFP (106°41.24′E, 29°37.42′N). The forest is located about 20 km in the northeastern position of Chongqing City, with an altitude from 200 to 550 m (Fig. S1). The mean annual precipitation of 1028 mm with 75% of the rainfall occurs from May to October. The mean annual air temperature is 18.2 ℃. The stand is homogeneous, dominated by Masson pine and some associated species such as camphor (*Cinnamom camphora*) and Gugertree (*Schima superba* Gardn. et Champ). Clay mineralogy is dominated by kaolinite and the soil is typically mountain yellow

© Author(s) 2019. CC BY 4.0 License.

earth (corresponding to an Acrisol in FAO) (Zhou et al., 2018). Detail of the Hg concentrations in the environment medium showed in the Supporting Information (SI, Supporting Text). The total area of the studied catchment was 1.06×10^3 ha in the TFP (Fig. S1).

2.2. Dynamic flux chamber measurement

Previous studies investigating soil-air Hg fluxes have been conducted only over several days or at a single plot. To reduce the influence of spatial uncertainty of Hg fluxes, different ecosystems were selected for study in a sub-catchment in the TFP of Chongqing, including a coniferous forest (plots A and B), a wetland (plot C), a broad-leaved (camphor) forest (plot D) and an open field with bare soil (plot E) (Fig. 1). To reduce the influence of temporal uncertainty of Hg fluxes, 130-day flux observations were undertaken over four seasons (about one-month of continuous observations for each season) in 2014. Plot A was positioned on the top of the hill slope; plot B was in the middle of the hill slope; plot C was in the wetland within a coniferous forest; plot D was in broad-leaved (evergreen) forest and plot E is in open field. Details of the plot instrumentation and sampling period can be found in the Table S1.

The DFC design and sampling methods are detailed in the SI. A sub-stream of air was trapped by a pair of gold quartz cartridges at a flow rate of 0.5 L min^{-1}, which was measured by an integrating volume flow meter. The soil Hg flux was calculated using the following equation:

$$F = (C_0 - C_i) \times Q/A \qquad (1)$$

where F is the soil Hg flux (ng m^{-2} hr^{-1}); C_o and C_i are the steady state Hg concentrations (ng m^{-3}) of the outlet and inlet air stream, respectively, which were calculated by the Hg mass detected in gold cartridges and the corresponding air volume; A is the surface area enclosed by the DFC; Q is the flow rate of ambient air circulated through the DFC (10 L min^{-1}). The pair of gold cartridges were collected twice a day: every morning (about 8:00) and afternoon (about 17:00) representing night (17:00−8:00 of next day) and day (8:00−17:00) emissions, respectively. Twenty gold quartz cartridges alternately used during the sampling. Additionally, diurnal variations of soil-air Hg fluxes were also conducted in each season, with gold cartridges collected every half an hour.

2.3. Empirical models of soil-air Hg fluxes.

The application of models has been used to estimate Hg emissions from soil to the atmosphere.

© Author(s) 2019. CC BY 4.0 License.

131 For this study, we extend the model developed from factorial simulation experiments by (Lin et al.,
132 2010) by modeling daily average Hg fluxes as a function of a number of environmental factors,
133 including the effects of solar radiation, soil temperature, soil Hg concentrations, atmospheric Hg
134 concentrations and soil moisture. For each plot, the datasets of fluxes measured by DFC and
135 corresponding environmental factors (meteorological parameters and soil parameters) from four
136 seasons were performed. If the individual environmental factors and the interaction terms were
137 determined to be significant, their effects were incorporated into a multivariate surface response
138 analysis to understand the process variability. This allowed for weighing the effects of
139 environmental conditions in the nonlinear regression analyses, which used the final predictive
140 models for Hg flux. Data analyses (estimate of effects and ANOVA) of the factorial experiments
141 were performed using Spss Statistics 17.0, and nonlinear regression analyses and their visualization
142 were performed using MATLAB with the Statistics Toolbox. Predictive models were developed
143 from daily flux observations with corresponding environmental factors in four land-cover categories:
144 coniferous forest (plot A), wetland (plot C), broad-leaved forest (plot D) and open field (plot E).
145
146 **2.4. Soil pore TGM measurement and diffusion coefficient**
147 The measurement of soil pore TGM was based on the method of Moore et al. (2011). Soil pore
148 gas samples were sequentially collected from inverted Pyrex glass funnels installed at different soil
149 horizons using a vacuum pump and Teflon tubing. The top diameter of the Pyrex glass funnel was
150 100 mm and the stem length was 100-mm. Mercury in soil pore gas was collected on the gold quartz
151 cartridges using a flow rate of 20 mL min^{-1}, which eliminated entrainment of ambient air and did
152 not disturb the soil pore gas profile (Mason et al., 1994;Sigler and Lee, 2006). Flows for each funnel
153 were controlled by a separate rotameter that was calibrated by mass flow rate meter at the beginning
154 and end of each sampling period. In the spring, soil pore TGM was measured at plots A and D at
155 depths of 3, 6 and 10 cm. In the subsequent summer, autumn and winter, soil pore TGM was
156 measured at plots A, B, D and E at five depths of Oe-Oa soil horizon interface (3 cm depth), the Oa-
157 A soil horizon interface (6 cm depth), 5 cm into the A soil horizon (10 cm depth), A2-B soil horizon
158 interface (20 cm depth) and 5 cm into the C soil horizon (50 cm) in each plot. Saturated soil water
159 precluded measurement of soil TGM at plot C (wetland) (Fig. 1).
160 Soil-air flux is the relationship of the dynamic diffusion between soil pore TGM concentrations

Atmos. Chem. Phys. Discuss., https://doi.org/10.5194/acp-2019-161
Manuscript under review for journal Atmos. Chem. Phys.
Discussion started: 18 March 2019
© Author(s) 2019. CC BY 4.0 License.

Atmospheric Chemistry and Physics Discussions

underneath the soil surface layer and TGM in atmosphere, suggesting that soil Hg^0 formation and diffusion influenced the soil-air flux. Based on a two-resistance exchange interface model and Fick's first law, the diffusive vertical soil flux, F (ng m^{-2} hr^{-1}), was calculated from the gradient of TGM concentration between soil air and the above atmosphere:

$$F = Ds\ \frac{C_S - C_a}{Z_j - Z_k} = Ds\frac{\Delta C}{\Delta Z} \quad (2)$$

where D_s is the overall Hg exchange coefficient of soil-air interface; F is the overall Hg exchange flux; C_s and C_a are the TGM concentrations in soil pore air and soil surface atmosphere; Z_j and Z_k are the soil layer depths.

2.5. Environmental Measurements.

At each sampling location, soil samples were collected from the DFC footprint (0−5 cm). Soil Hg and organic matter (SOM) concentrations were determined. Soil percent moisture and temperature were monitored with Time Domain Reflectometry (TDR) Hydra Probe II (SDI−12/RS485) and a Stevens water cable tester (USA). Solar radiation was collected with a weather station (Davis Wireless Vantage VUE 06250 Weather Station, Davis Instruments, Hayward, CA) located in the TFP Forest Station about 500 m away from the plots. The total Hg concentration in the soil samples was determined using a DMA-80 direct Hg analyzer (Milestone Ltd., Italy) and SOM content in soils was determined using the sequential loss on ignition (LOI) method (Zhou et al., 2013). Detail of the measurements showed in the SI. Quality Assurance and Quality Control (QA/QC) measures for the recovery, collection efficiency and parallelism of the gold cartridges before and after the campaign, and for soil Hg determination are also detailed in the SI.

3. Results and discussion

3.1. Landscape- and Forest Species-Dependence of Soil-Air Hg Fluxes at the Forest Catchment Scale

The soil TGM flux measurements for the five plots were calculated for the day and night, and reported as mean daily fluxes with standard deviations (SD) (Fig. 2). Over the course of the campaigns, net TGM emission was observed at the open field, coniferous forest and the broad-leaved forest, while net deposition was evident at the wetland, with corresponding fluxes (mean ±

© Author(s) 2019. CC BY 4.0 License.

SD) of 24 ± 33, 3.5 ± 4.2, 2.8 ± 3.9, 0.18 ± 4.3 and −0.80 ± 5.1 ng m^{-2} hr^{-1}, respectively. This pattern suggests that soil-air Hg fluxes at catchment scale vary by soil properties (including soil parent materials) and forest species composition. High variability (SD and coefficient of variation (SD/mean, range of 119−2374%)) was evident in daily Hg fluxes, largely driven by meteorological variation, demonstrating that measurement of several days may exist a large difference with long-term study that should be undertaken to reduce the uncertainty of temporal patterns.

The mean TGM flux in open field was about 8.6 times higher than that under the forest canopy ($p < 0.001$). Our results are consistent with Ma et al. (2013) and Xin and Gustin (2007), showing large Hg evasion following forest conversion to bare soils due to direct exposure to sunlight, where fluxes were enhanced by solar radiation and temperature. Due to frequent heavy rains in the catchment, large amount of surface runoff converged to the wetland (plot C). Therefore, Hg and SOM in surface soils were eroded by runoff, which resulted in low soil Hg concentration (Table 1) and the lowest fluxes of the plots studied (overall net sinks). In addition, soils were mostly saturated throughout the year, limiting fluxes from the wetlands and likely contributing to the sink behavior, which was consistent with the Kyllonen et al. (2012) and Lindberg et al. (1998), suggesting the wet conditions can inhibit the flux. In the broad-leaved (camphor) forest (plot D), litterfall deposition was twice as high as that in the coniferous (pine) forest (plot A and B) (Zhou et al., 2018), resulting in greater shielding of sunlight to the surface soil and limiting soil Hg evasion, because sunlight can both increase solar radiation and soil temperature, which can enhance the photochemical reduction of Hg^{2+} on soil surface and Hg^0 evasion after its formation from Hg^{2+}, respectively. Moreover, some studies have reported significantly higher Hg inputs with a larger fraction occurring as throughfall fluxes from conifers than hardwoods (Blackwell et al., 2014). Throughfall Hg is likely more reactive than litter Hg (Renner, 2002) and subsequently higher inputs and throughfall fraction could contribute to higher Hg evasion from the coniferous (pine) forest. In the middle of the pine hill slope (plot B), soil Hg concentration was elevated compared to the upslope plot (Table 1), corresponding with higher soil Hg fluxes. The forest canopy not only influences the soil Hg concentration by atmospheric Hg deposition, but also alters soil physio-chemical properties (e.g. SOM, pH, porosity) which affect soil-air exchange. For example, the annual litterfall Hg deposition flux at the broad-leaved forest (91 μg m^{-2} yr^{-1}) was approximately two times greater than the coniferous forest (41 μg m^{-2} yr^{-1}) (Zhou et al., 2018); conversely, the SOM and soil Hg concentration in the broad-leaved forest were

Atmos. Chem. Phys. Discuss., https://doi.org/10.5194/acp-2019-161
Manuscript under review for journal Atmos. Chem. Phys.
Discussion started: 18 March 2019
© Author(s) 2019. CC BY 4.0 License.

lower than the coniferous forest. Moreover, litter decomposition rate was lower, but Hg accumulation rate was much higher in the coniferous forest compared to the broad-leaved forest (Zhou et al., 2018), which resulted in seemingly inconsistent patterns between litterfall mass and SOM, as well as litterfall Hg deposition and soil Hg concentrations. Tree species can change soil physicochemical properties (e.g. SOM, soil Hg concentrations) as we stated above, which influences the soil-air exchange, contributing to much lower TGM evasion in the broad-leaved forest than the coniferous forest (Fig. 2).

Based on the areal distribution of each plot type (coniferous upland and mid-slope, broad-leaved, wetland, open) in the study sub-catchment (4.6 ha) (Table S1), the area-weighted TGM flux was 3.2 ng m^{-2} hr^{-1} for the whole forest catchment. The observations from the campaigns in this study should reduce the overall uncertainty associated with soil-air fluxes of TGM in the forest catchment. Previous studies have generally measured soil TGM fluxes at only one location or in a single forest stand to characterize the whole ecosystem. However, our observations clearly show that soil-air Hg fluxes differ substantially across different plots in this study, indicating that forest type and landscape position significantly affect the TGM fluxes between soil and atmosphere.

Soil TGM fluxes not only exhibited clear seasonal variations at all the plots, but also were responsive to seasonal and meteorological patterns. The fluxes were generally highest in the summer (Fig. 2), which showed net emissions at all the five plots, followed by spring, autumn, with the lowest values in the winter, which exhibited net deposition at all plots with the exception of plot B. The observed seasonal variation was dependent on sunlight because solar radiation drives photochemical reduction of Hg^{2+} (note correlation between the TGM fluxes and solar radiation, Fig. S2). Additionally, greater solar radiation increases temperature, which promotes the production of soil Hg gas by biological and thermal processes (discussed in detail in the next section). We also observed strong variation in TGM evasion under different weather conditions. For example, the fluxes were highly variable across the seasons; area-weighted fluxes for the catchment were 4.26, 7.61, 1.24 and −0.31 ng m^{-2} hr^{-1} in spring, summer, autumn and winter, respectively. Therefore, if soil TGM fluxes were only made for one or two seasons, estimates of annual fluxes could be highly biased. For example, summer only measurements of TGM evasion would greatly overestimate annual values. Other environmental factors also significantly influenced the soil-air fluxes. For example, rain events strongly decreased TGM fluxes at all plots (Fig. S3). Therefore, long-term

© Author(s) 2019. CC BY 4.0 License.

observations reduce the uncertainties and bias of temporal patterns of soil-air Hg fluxes and multi-plot observations reduce the uncertainties and bias in spatial analysis and improve overall ecosystem estimates soil evasion compared to previous studies.

3.2. Correlations between Environmental Factors and Fluxes

According to a global database, atmospheric fluxes at Hg-enriched sites are positively correlated with substrate Hg concentrations, but this relationship is not observed at background sites (Agnan et al., 2016). The soil Hg fluxes were strongly correlated with soil Hg concentrations at vegetated sites (forests and wetland) of the TFP ($r^2 = 0.97$, $p<0.01$, Fig. S4).

Solar radiation was found to significant increase TGM fluxes in each plot, because photo-reduction is a major driver of TGM evasion from earth surface (Howard and Edwards, 2018;Park et al., 2014;Kuss et al., 2018;Song et al., 2018), which was more obvious in the open field due to greater solar radiation (Fig. S2). The fluxes in the wetland (plot C) were less strongly correlated with soil temperature compared to the other plots ($p<0.01$ for plot C and $p<0.001$ for the other plots, Fig. S5). Generally, temperature is an important factor that promotes Hg^0 evasion after its formation from Hg^{2+} by biotic and abiotic processes in soils (Pannu et al., 2014). However, the wetland soil was largely saturated. This condition likely blocked soil pore TGM release to the atmosphere, resulting in the weaker correlation between soil temperature and the fluxes.

During the campaign, significant negative correlations were evident between soil moisture and soil-air fluxes of TGM at the five plots ($r^2= 0.03−0.39$, $p<0.05$ for all, Fig. S6). Generally there is an optimum soil moisture condition that maximizes soil TGM flux (Gustin and Stamenkovic, 2005;Lin et al., 2010;Obrist et al., 2014;Pannu et al., 2014), which ranges from 60% to 80% of a soil's water holding capacity (Pannu et al., 2014). A laboratory experiment using undisturbed soil collected from the TFP study area showed that increasing soil moisture from 2% to 20% increased the TGM flux 80% at 24 °C (Wang et al., 2014). A second field experiment was conducted to study the effects of soil moisture on TGM flux at the TFP, showing that increasing soil moisture gradually decreased the soil Hg emissions over the range of 31−39% (Zhou et al., 2017b). Combining these experiments, the soil Hg fluxes in the forest catchment should increase from low values of soil moisture reaching an optimum in the range of 20-30% and then decreasing with increasing soil moisture above these values. Perennially humid weather results in relatively high soil moisture in

© Author(s) 2019. CC BY 4.0 License.

the subtropical forest (largely >25% during the campaigns). Considering the relatively high bulk density and low porosity of soil at the TFP (Sørbotten, 2011), soil moisture likely exceeded the optimum range for TGM evasion during the campaigns resulting in significantly negative correlations (Fig. S6).

Soil-air Hg fluxes showed significant negative correlations with atmospheric TGM concentrations at the five plots (r^2= 0.03−0.26, $p<0.05$, Fig. S7). According to the two-resistance exchange interface model, the exchange fluxes are controlled by the gradient of TGM concentrations at both interfaces (Zhang et al., 2002), and therefore elevated atmospheric TGM concentrations should decrease the diffusion of soil pore TGM to the atmosphere. These results are consistent with our experiment in this forest, where artificially increasing ambient-air TGM concentrations significantly inhibited soil Hg volatilization (Zhou et al., 2017b).

Diurnal variation in soil-air TGM flux were observed at plot A (Fig. 3). Soil TGM fluxes were well correlated with soil and air temperature ($p<0.01$ for all) and were highly dependent on solar radiation in spring, summer and autumn ($p< 0.01$ for all) but not in winter ($p> 0.05$), which are similar to patterns from other studies (Agnan et al., 2016;Obrist et al., 2010). Solar radiation has been shown to promote photochemical reduction of soil-bound Hg and enrich Hg in soil pore gas. This reaction is also kinetically enhanced at higher temperatures (Eckley et al., 2015;Gustin et al., 2002;Lin et al., 2010;Zhang et al., 2001). Compared to the other three seasons, the relatively low soil temperature (5.95 °C) may have limited the relationship between soil TGM flux and solar radiation during the winter season.

3.3. Estimation of Hg mass-balance

To investigate the process of Hg budget, the flux of Hg input (atmospheric deposition) and the flux of Hg output from the forest soils (air-to-air emission, leaching to surface and underground runoffs) were calculated (Fig. 1). The total Hg input includes litterfall deposition and throughfall deposition. According to the previous study, the annual litterfall and deposition fluxes of Hg were about 40.5 μg m^{-2} (Zhou et al., 2018) and 67.5 μg m^{-2} (Luo et al., 2015) in the in the study sub-catchment. Thus, annual Hg input (litterfall + throughfall) to the forest was 108 μg m^{-2}.

The dominate output pathways of Hg from forest were surface runoff, underground runoff and soil-air Hg flux. The amount of surface runoff and underground runoff, which are assumed to be 25%

© Author(s) 2019. CC BY 4.0 License.

rainfall amount (Liu, 2005) and 50% throughfall amount (Luo et al., 2015) and the Hg concentrations in surface runoff and underground runoff were 6.2 ng L^{-1} (Wang et al., 2009) and 21.8 ng L^{-1}.(Zhou et al., 2015) The annual output fluxes from underground runoff and surface runoffs was 6.0 and 2.4 μg m^{-2}, which was roughly estimated according to the Hg concentration in runoffs and their volumes in TFP. Therefore, the total output of Hg (surface runoff + underground runoff + soil-air Hg exchange flux) was 36.4 μg m^{-2} yr^{-1}. The total Hg retention in forest soil (input − output) was 71.6 μg m^{-2} yr^{-1}, accounting for 66% of the total Hg depositions, suggesting that forest soils in the southwestern China are net sinks for atmospheric Hg.

3.4. Development of Empirical Models for Hg Flux from Soils

Predictive models were developed from multivariate regression analysis using the soil-air Hg fluxes and environmental parameters measured at the five plots. Over the last decade, studies have established empirical equations of soil Hg fluxes using one or several parameters, but have not considered air TGM concentrations as a controlling parameter. The empirical equations which utilize different combinations of parameters are summarized in Table S2. Based on our soil TGM flux data and the two-layer diffusion model (Zhang et al., 2002), air TGM concentrations should not be ignored in estimating TGM evasion in forest soils from the region and were used in the regression analysis to ensure the model's applicability. Four predictive models were developed from multivariate regression analysis using the Hg fluxes measured by DFC for different ecosystems grouped into the four land-cover categories: coniferous forest, wetland, broad-leaved forest and open field. Our flux factorial experiments and multivariate response analysis considered quadratic interactions of the environmental parameters considered.

$$F = (a \times S_c) \times [\partial_0 + \partial_1 T + \partial_2 W + \partial_3 L + \partial_4 C_a + \partial_5 (T \times W) + \partial_6 (T \times L) + \partial_7 (T \times C_a) + \partial_8 (W \times L) + \partial_9 (W \times Ca) + \partial_{10} (L \times C_a) + \partial_{11} T^2 + \partial_{12} W^2 + \partial_{13} L^2 + \partial_{14} C_a{}^2] \quad (3)$$

where a is the scaling factor of soil Hg emission; S_c is soil Hg concentration (ng g^{-1}); W is soil moisture (wt %); L is the fraction of solar radiation attenuated by leaf canopy before reaching to the ground (W m^{-2}), which is parametrized by leaf area index (LAI) in different forest ecosystems (Wang, 2012); C_a is ambient air TGM concentrations (ng m^{-3}); T is soil temperature (ºC); and ∂_i is the coefficients of predictors (i = 0−14). The soil Hg concentration was one of the most important parameters driving soil TGM emissions (Gbor et al., 2006;Lin et al., 2010). In this empirical

© Author(s) 2019. CC BY 4.0 License.

approach soil Hg is multiplied by scaling factor obtained from Fig. S4 (a = 2.8 × 10^{-2} g m^{-2} hr^{-1}), similar to the approach used by Kikuchi et al. (2013). All the soil parameters were measured in the soil depth of 5 cm.

The four different sets of model coefficients were derived separately from the flux data from the field-observation experiments. The number of daily flux observations with corresponding environmental factors used to establish the models were 124, 127, 135 and 102 for the coniferous forest (plot A), the wetland, the broad-leaved forest and the open field, respectively. Regression coefficients for these plots and the whole sub-catchment are shown in Table S3. To simplify the models, ten coefficients were used for each plot based on the principal component analysis (PCA). The estimated mean flux values were 3.92 ± 3.13, 4.20 ± 3.55, −0.88 ± 1.12, 0.14 ± 2.38, 23 ± 30 ng m^{-2} hr^{-1}, which were comparable to the measured fluxes of 3.5 ± 4.2, 2.8 ± 3.9, −0.80 ± 5.1, 0.18 ± 4.3 and 24 ± 33 ng m^{-2} hr^{-1} for the plots A to E.

The performance of the models was compared against measured soil flux data (Fig. 4). Normalized Hg flux (predicted using equation 3) agreed well with the measured flux for different ecosystems, with most scatter plots of predicted fluxes falling within the 95% confidence interval (Fig. S8). The cumulative fluxes estimated from the predicted and measured flux was less than 15% different for all ecosystems. The scatter plots showed strong correlations (r^2 = 0.28 to 0.70, Fig. S8) between the measured and predicted fluxes, although the variability of measured fluxes was greater than estimated values. The model was capable of depicting the observed seasonal patterns of soil Hg fluxes with < 5% difference between the measured and predicted values.

To date we have had limited opportunity to validate the empirical model predictions. The performance of the empirical model developed for the pine plot A was tested using the data from pine plot B that was not used in developing the empirical model. The model-estimated fluxes of soil TGM for plot B are consistent with measured values using the DFC (Fig. 4). This analysis gives us some confidence in model performance. The multivariate response analysis has improved our ability to estimate soil Hg fluxes. However, further model verification is still needed when additional soil TGM flux data become available, particularly using data from other field study sites.

3.5. TGM in Soil Vertical Profiles

Contour plots of soil pore TGM concentrations measured at multiple soil depths and above

Atmos. Chem. Phys. Discuss., https://doi.org/10.5194/acp-2019-161
Manuscript under review for journal Atmos. Chem. Phys.
Discussion started: 18 March 2019
© Author(s) 2019. CC BY 4.0 License.

ground for the four plots (A, B, D and E) are shown in Fig. 5. Mean soil pore TGM concentrations for all depths were significantly higher in the open field (15.8 ± 11.9 ng m^{-3} for plot E), than the Coniferous forest (11.4 ± 10.1 and 12.0 ± 7.83 ng m^{-3} for plots A and B, respectively). These plots were significantly higher than the broad-leaved forest values (6.73 ± 3.81 ng m^{-3} for plot D). Soil pore TGM concentrations exhibited clear seasonal variations at soil depths at all the sampling plots. The highest mean TGM concentration was observed in summer, followed by spring and autumn, with the lowest mean concentration in winter. Within each study plot, pore TGM concentrations increased with increases in soil temperature (Table S4), which appears to be an important factor driving the seasonal variation. Soil pore TGM production occurs from the reduction of Hg^{2+} by biotic and abiotic processes. In a laboratory study of boreal forest soils, Pannu et al. (2014) observed that soil Hg converted to Hg^0 via biotic processes was more than five times greater than that derived by abiotic processes, and biotic reduction was more pronounced with temperatures increases. Thus it can be inferred that temperature is an important factor casing in seasonal variation of soil pore TGM concentrations, given limited light penetration to soil depths.

Over the entire campaign at the top three soil pore sampling depths in each of the four plots, soil moisture was consistently negatively correlated with pore TGM concentrations (Table S4). There is an optimum soil moisture that facilitates pore TGM production, as discussed above. A laboratory study demonstrated increases in soil Hg^0 concentrations with increases in soil moisture from 15% to 60% water filled pore space, with no Hg^0 formation above 80% (Pannu et al., 2014). Additionally, given that soil Hg conversion to Hg^0 is mainly via biotic processes, maximum aerobic microbial activity was delineated with soil water content equivalent to 60% of a soil's water holding capacity (Breuer et al., 2002;Kiese and Butterbach-Bahl, 2002). Similarly, Obrist et al. (2014) found higher pore TGM concentrations under 25 to 35% soil moisture than for 10 to 20% or 35 to 45% soil moisture in pine forests of California, U.S. At the TFP, more than 95% of soil moisture values exceeded 20%, which may exceed the optimum for soil Hg^0 production, resulting in the inverse correlations.

Sigler and Lee (2006) demonstrated that pore TGM concentrations was significantly correlated with soil Hg concentrations in soil profiles at a forested plot. However, this result is not consistent with our observations. We find that soil pore TGM varies more with varying environmental conditions that soil Hg. We observed vertical TGM gradients in soil during different seasons. In the

© Author(s) 2019. CC BY 4.0 License.

coniferous forest in spring, the highest pore TGM occurred at a depth of 6 cm. During the other three seasons, the highest mean pore TGM was at 10-cm depth, with values decreasing to the soil surface and the lower layers. In the broad-leaved forest in spring and summer, the highest pore TGM concentrations occurred at top soil layer (3cm), and decreased with soil depth. In autumn and winter, the pore TGM concentrations were uniform at the five soil depths. In the open field in summer, the highest pore TGM concentrations occurred at a depth of 6 cm. In autumn and winter, the pore TGM concentrations decreased with depth to 10 cm and were uniform at the three lower depths. With the exception of plots A, D and E in winter, TGM concentrations at 3 cm exceeded values in soil surface air.

Soil Hg concentration and SOM were measured at each sampling depth of each plot (Fig. S9). In the forest ecosystem, Hg concentrations were significantly correlated with SOM, with the highest values in the organic layer. Both Hg concentrations and SOM significantly decreased with soil depth, but did not change below depths of 10 cm in the soil profiles. In the open field (plot E), the highest Hg concentrations were found between 10 and 20 cm, with lower Hg concentrations at shallower and deeper depths and Hg concentrations did not vary with SOM likely because of agricultural cultivation. SOM is known to play a central role in the storage and immobilization of Hg in soils (Grigal, 2003;Zhou et al., 2017b). The dominant soil Hg form, Hg^{2+} strongly binds to organic matter through complexation with thiol ligands (Zhou et al., 2015). Although much higher Hg concentrations were evident at the upper layers, it was likely tightly bound to SOM limiting conversion from Hg^{2+} to Hg^0 by biotic and abiotic processes. Additionally, Schlüter (2000) demonstrated that oxidation of Hg^0 to Hg^{2+} may proceed at a reduction-oxidation potential lower than its half-reaction due to strong binding of Hg^{2+} to organic matter. Our field study in the coniferous forest (Zhou et al., 2017b) and previous sorption studies (Eckley et al., 2011;Fang, 1978) also showed that Hg^0 is adsorbed rapidly to surface soils under high air Hg^0 exposure. In the coniferous forest, the mean SOM decreased from 137.6 at the surface to 58.0 g kg^{-1} at depth, while the pore TGM concentrations increased from 9.44 to 14.63 ng m^{-3} in the interval of 3 cm. Thus, Hg^0 produced at surface layers or transported from deeper soil layers may be re-oxidized or absorbed by SOM in the surface soil. Although a similar SOM pattern was evident in the soil profiles of the broad-leaved forest, the highest pore TGM concentrations occurred in surface soils. The surface SOM of the broad-leaved forest (67.9 g kg^{-1} at 3 cm) was half of the value at the coniferous forest

© Author(s) 2019. CC BY 4.0 License.

(137.6 g kg^{-1}), while the soil Hg concentration was highest at this surface layer. The higher Hg to SOM ratio at the broad-leaved forest may have contributed to greater surface pore TGM production, due to less immobilization of Hg^0 from the lower concentrations of SOM.

Lower pore TGM concentrations in the broad-leaved forest than the coniferous forest may be indicative of smaller spatial variability in soil pore TGM profiles, possibly due to local differences in porosity, SOM and Hg concentrations. In the open field, the vertical profiles of pore TGM may be influenced by direct solar radiation that increases soil temperature of the upper layers. When surface soil temperature in autumn and winter decrease, the vertical TGM profile is dominated by soil Hg concentration. In all plots during all four seasons, comparable TGM concentrations were observed between 20 and 50 cm, which may be due to comparable physicochemical properties in lower mineral horizons (e.g. Hg concentrations, SOM, Fig. S9).

Although other studies have shown different TGM patterns than observed in our study (Moore and Castro, 2012;Obrist et al., 2014;Sigler and Lee, 2006), these measurements seem to support our observations of TGM production. For example, the soil pore TGM concentrations were highest and most variable in the O- and upper A-horizons of forest soils, with soil moisture, temperature and SOM significantly affecting TGM concentrations. Soil pore TGM concentrations at the TFP were much higher than values reported in previous studies, which showed concentrations ranging from the detection limit to 8 ng m^{-3} in upper soils and were generally less than 2 ng m^{-3} from 20 to 50 cm of the soil profile (Moore and Castro, 2012;Sigler and Lee, 2006). Sigler and Lee (2006) and Obrist et al. (2014) observed the highest pore TGM concentrations in the upper organic soil and litter layers, which is inconsistent with our observation of maximum TGM concentrations in the upper mineral soil (depth 6−10 cm) in the coniferous forest. Previous studies have also shown the highest pore TGM concentrations observed in the upper mineral soil layers (Obrist et al., 2014). Our observations and above studies show a near-surface source of TGM from soil evading to the atmosphere. Observations of pore TGM concentrations decreasing in lower layers supports a TGM sink in mineral soils. Obrist et al. (2014) defined an Hg^0 immobilization concept for soils, in which pore TGM concentrations in lower horizons are below values in the upper horizons. In the forest plots at the TFP, the annual average soil pore TGM concentrations at 10, 20 and 30 cm were all below concentrations in the upper horizons; suggesting immobilization of TGM in the mineral soil, a pattern consistent with the study of two pine forests in California, U.S. (Obrist et al., 2014). However,

© Author(s) 2019. CC BY 4.0 License.

460 for the open field in the current study, TGM formation mostly occurred in mineral soils because of
461 higher soil Hg concentrations in the mineral horizons as we stated above, which may facilitate the
462 mineral pore TGM diffusion to surface soil horizon and the emission flux. Another major objective
463 of the soil pore TGM study was to investigate the relationship between TGM in vertical soil pore
464 profiles and the ultimate diffusion of TGM from the soil surface. No relationship was found between
465 soil pore TGM flux and soil pore TGM concentrations at 20 or 50 cm. However, soil TGM fluxes
466 were strongly correlated with soil pore TGM concentrations or the gradient between soil pore
467 concentrations at 2, 5 and 10 cm depths and the atmosphere (Table S4 and Fig. S10). TGM
468 concentrations were highest at these surface depths and values decreased with greater depth,
469 suggesting that production and subsequent emission of Hg from soil was derived from the upper 10-
470 cm depths. Similar observations by Sigler and Lee (2006) showed that Hg emissions originated from
471 shallow (5 cm) depths in forest soils due to highest soil pore TGM produced in surface horizons.
472 We also investigated the role of vertical profiles of pore TGM in diffusion from the soil column.
473 In the equation 2, ΔC and F was not only from the diffusion of pore TGM produced in the soil profile,
474 but also could be derived from photochemical reduction of Hg^{2+} on soil surface in daytime. We
475 estimated the diffusion coefficient between the soil at 3 cm and the atmosphere in daytime ($D_{s\ day}$),
476 nighttime ($D_{s\ night}$) and whole day ($D_{s\ day+\ night}$). The estimated $D_{s\ day}$, $D_{s\ night}$ and $D_{s\ day+\ night}$ were
477 0.015, 0.013 and 0.014 $m^2\ hr^{-1}$ for plot A and 0.0098, 0.0096 and 0.0097 $m^2\ hr^{-1}$ for plot B in the
478 coniferous forest, and 0.010, 0.0076 and 0.0079 $m^2\ hr^{-1}$ for plot C in the broad-leaved forest,
479 respectively. However, we found the TGM diffusion coefficient was 23 times higher in the daytime
480 ($D_{s\ day}$: 0.099 $m^2\ hr^{-1}$) than for nighttime ($D_{s\ night}$: 0.0095 $m^2\ hr^{-1}$) for the open field, with $D_{s\ day+\ night}$
481 of 0.0408 $m^2\ hr^{-1}$. Note that, in the open field, the $D_{s\ night}$ was comparable to those in forest plots,
482 but the $D_{s\ day}$ was significantly higher. These data suggest that the formation of Hg^0 in the surface
483 soil exposed to solar radiation directly overestimated TGM D_s in soil. Therefore, to avoid the photo-
484 reduction of Hg^{2+} in daytime, we posit that $D_{s\ night}$ can represent the local diffusion coefficient (D_s)
485 (Fig. 6) and be used in future model development.
486 Physicochemical properties of soils have a significant effect on the pore gas production and
487 transport, especially porosity and humidity (Prajapati and Jacinthe, 2014;Ryzhakova, 2014). In the
488 same coniferous stand, the soil TGM diffusion coefficient was much higher at plot A (0.013 $m^2\ hr^{-1}$)
489 than plot B (0.0.0096 $m^2\ hr^{-1}$). This difference may be related to the higher SOM at plot B. The

© Author(s) 2019. CC BY 4.0 License.

higher SOM could immobilize TGM in the upper soil as discussed above, mitigating pore TGM diffusion to the atmosphere. Compared to other gases, for example, Ryzhakova (2014) showed that the D_s of radon ranged from 0.00050 to 0.0088 m^2 hr^{-1} for natural soils and the D_s for Sulphur hexafluoride for the peat cores ranged between 0.00032 to 0.0044 m^2 hr^{-1},[55] which were comparable with the D_s of Hg in our study.

4. Conclusion and implication

Through multi-plot and longer-term measurements, we were able to reduce the uncertainty of soil-atmosphere TGM fluxes at the catchment scale and obtain a better understanding of how landscape attributes contribute to the variability in soil Hg evasion. Empirical models of soil-air exchange fluxes were developed from multivariate regression analysis using the Hg fluxes measured by the DFC and environmental factors for different landscape conditions in a forest catchment. The observed DFC fluxes were significantly correlated to the first-order and second-order terms of environmental factors, including soil Hg concentration, soil moisture, solar radiation, air TGM concentration, soil temperature. In particular, we found that atmospheric TGM concentrations at TFP significantly affect TGM diffusion form soil pore according to the two-resistance exchange interface model.

The developed model can be used to examine how soil Hg fluxes may be impacted by changes in environmental conditions such as temperature, soil moisture or concentrations of atmospheric TGM. For example, if the atmospheric TGM decreased to a uniform 0.1 ng g^{-1}, the Hg area-weighted emission flux is projected to increase up to 5.0% in the forest and 0.5% in the open field, respectively. The empirical models presented in this study demonstrate a promising approach to better estimate Hg exchange between the atmosphere and soil, significantly improving the accuracy of these estimates due to the consideration of important controlling environmental factors. Additional data from additional sites which represent wider range of substrates and environmental conditions in different terrestrial ecosystems are needed to verify the empirically modeling framework we propose.

Another implication of our results is that Hg in upper mineral layers would migrate to lower mineral horizons through pore TGM diffusion, although this pathway may small compared with

© Author(s) 2019. CC BY 4.0 License.

520 rainwater infiltration and immobilization (Jiskra et al., 2015). For instance, throughfall Hg
521 deposition was 67.5 μg m^{-2} yr^{-1} in the coniferous forest in our study area (Luo et al., 2015) and the
522 percolation of Hg via soil solution through the surface litter layer into the mineral soil layer has been
523 estimated at 33 μg m^{-2} yr^{-1} (Schwesig and Matzner, 2001). Thus, transport and immobilization of
524 soil pore TGM to the lower mineral soil is likely to be much smaller than by the drainage pathway.
525 In each season, soil Hg flux was strongly correlated with pore TGM concentrations at 3 cm and less
526 strongly correlated than values at other depths (Table S4), suggesting that reduction and terrestrial
527 Hg^0 losses would occur within the upper surface soil horizons, with limited loss from deeper mineral
528 soils. The large Hg pools in mineral soils (accounting for 94.1% of the total over 0−40 cm) (Zhou
529 et al., 2016) were not only derived from soil water percolation but also with a contribution from
530 TGM diffusion from upper soils. Compared to Hg concentrations of mountain yellow earth soil
531 measured in 1980s in Chongqing China (59 ng g^{-1}) (Chen, 1982), the average Hg concentration in
532 the mineral horizons (85 ng g^{-1}, 6~50 cm) in our study increased about 44%.
533
534 ***Author contributions.*** JZ performed the field observation. ZWW and XSZ designed the
535 experiments and assisted with the initial instrument installation. CTD and CJL assisted with
536 scientific analysis. JZ prepared the manuscript with significant contributions from all of co-authors.
537
538 ***Competing interests.*** The authors declare that they have no conflict of interest.
539
540 **ACKNOWLEDGEMENTS**
541 This work was funded by the Natural Science Foundation of China (No.41371461 and No.
542 41673113), the National Basic Research Program of China (973 Program; 2013CB430002), and
543 "Strategic Priority Research Program" of the Chinese Academy of Sciences (grant XDB14020205).
544 The authors would like to thank Mingquan Zou for his assistance in field works.
545
546 **References**
547 Agnan, Y., Le, D. T., Moore, C., Edwards, G., and Obrist, D.: New constraints on terrestrial surface-
548 atmosphere fluxes of gaseous elemental mercury using a global database, Environmental Science
549 & Technology, 50, 507−524, 10.1021/acs.est.5b04013, 2016.
550 Blackwell, B. D., Driscoll, C. T., Maxwell, J. A., and Holsen, T. M.: Changing climate alters inputs and

© Author(s) 2019. CC BY 4.0 License.

pathways of mercury deposition to forested ecosystems, Biogeochemistry, 119, 215-228, 10.1007/s10533-014-9961-6, 2014.

Breuer, L., Kiese, R., and Butterbachbahl, K.: Temperature and moisture effects on nitrification rates in tropical rain-forest soils, Soil Science Society of America Journal, 66, 399-402, 2002.

Chen, Y.: Distribution of mercury in soils in Chongqing area, Chongqing Environmental Protection, 4, 106-113. In Chinese., 1982.

Eckley, C. S., Gustin, M., Miller, M. B., and Marsik, F.: Scaling non-point-source mercury emissions from two active industrial gold mines: influential variables and annual emission estimates, Environmental Science & Technology, 45, 392-399, 2011.

Eckley, C. S., Blanchard, P., Mclennan, D., Mintz, R., and Sekela, M.: Soil–air mercury flux near a large industrial emission source before and after closure (Flin Flon, Manitoba, Canada), Environmental Science & Technology, 49, 9750-9757, 2015.

Fang, S. C.: Sorption and transformation of mercury vapor by dry soil, Environmental Science & Technology, 12, 285-288, 1978.

Gbor, P. K., Wen, D., Meng, F., Yang, F., Zhang, B., and Sloan, J. J.: Improved model for mercury emission, transport and deposition, Atmospheric Environment, 40, 973-983, 2006.

Grigal, D. F.: Mercury sequestration in forests and peatlands: a review, Journal of Environmental Quality, 32, 393, 2003.

Gustin, M. S., Biester, H., and Kim, C. S.: Investigation of the light-enhanced emission of mercury from naturally enriched substrates, Atmospheric Environment, 36, 3241-3254, 2002.

Gustin, M. S., and Stamenkovic, J.: Effect of watering and soil moisture on mercury emissions from soils, Biogeochemistry, 76, 215-232, 2005.

Howard, D., and Edwards, G. C.: Mercury fluxes over an Australian alpine grassland and observation of nocturnal atmospheric mercury depletion events, Atmospheric Chemistry and Physics, 18, 129-142, 10.5194/acp-18-129-2018, 2018.

Jiskra, M., Wiederhold, J. G., Skyllberg, U., Kronberg, R. M., Hajdas, I., and Kretzschmar, R.: Mercury deposition and re-emission pathways in boreal forest soils investigated with hg isotope signatures, Environmental Science & Technology, 49, 7188-7196, 2015.

Kiese, R., and Butterbach-Bahl, K.: N2O and CO2 emissions from three different tropical forest sites in the wet tropics of Queensland, Australia, Soil Biology & Biochemistry, 34, 975-987, 2002.

Kikuchi, T., Ikemoto, H., Takahashi, K., Hasome, H., and Ueda, H.: Parameterizing soil emission and atmospheric oxidation-reduction in a model of the global biogeochemical cycle of mercury, Environmental Science & Technology, 47, 12266-12274, 2013.

Kuss, J., Krueger, S., Ruickoldt, J., and Wlost, K.-P.: High-resolution measurements of elemental mercury in surface water for an improved quantitative understanding of the Baltic Sea as a source of atmospheric mercury, Atmospheric Chemistry and Physics, 18, 4361-4376, 10.5194/acp-18-4361-2018, 2018.

Kyllonen, K., Hakola, H., Hellen, H., Korhonen, M., and Verta, M.: Atmospheric Mercury Fluxes in a Southern Boreal Forest and Wetland, Water Air and Soil Pollution, 223, 1171-1182, 10.1007/s11270-011-0935-1, 2012.

Li, Z. G., Feng, X., Li, P., Liang, L., Tang, S. L., Wang, S. F., Fu, X. W., Qiu, G. L., and Shang, L. H.: Emissions of air-borne mercury from five municipal solid waste landfills in Guiyang and Wuhan, China, Atmospheric Chemistry & Physics, 10, 3353-3364, 2010.

Lin, C. J., Gustin, M. S., Singhasuk, P., Eckley, C., and Miller, M.: Empirical models for estimating

© Author(s) 2019. CC BY 4.0 License.

mercury flux from soils, Environmental Science & Technology, 44, 8522-8528, 2010.

Lindberg, S. E., Hanson, P. J., Meyers, T. P., and Kim, K. H.: Air/surface exchange of mercury vapor over forests - The need for a reassessment of continental biogenic emissions, Atmospheric Environment, 32, 895-908, 10.1016/s1352-2310(97)00173-8, 1998.

Liu, H.: Dynamics of soil properties and the effects factors among secondary successive communities in Mt. Jinyun, Doctor's dissertation, Southwest Agricultural University, Chongqing, pp. 1-117 pp., 2005.

Luo, Y., Duan, L., Xu, G., and Hao, J.: Inhibition of mercury release from forest soil by high atmospheric deposition of Ca(2)(+) and SO(4)(2)(-), Chemosphere, 134, 113-119, 10.1016/j.chemosphere.2015.03.081, 2015.

Ma, M., Wang, D., Sun, R., Shen, Y., and Huang, L.: Gaseous mercury emissions from subtropical forested and open field soils in a national nature reserve, southwest China, Atmospheric Environment, 64, 116-123, 2013.

Mason, R. P., Fitzgerald, W. F., and Morel, F. M. M.: The biogeochemical cycling of elemental mercury: Anthropogenic influences, Geochimica Et Cosmochimica Acta, 58, 3191-3198, 1994.

Moore, C. W., Castro, M. S., and Brooks, S. B.: A simple and accurate method to measure total gaseous mercury concentrations in unsaturated soils, Water Air & Soil Pollution, 218, 11-11, 2011.

Moore, C. W., and Castro, M. S.: Investigation of factors affecting gaseous mercury concentrations in soils, Science of the Total Environment, 419, 136-143, 2012.

Obrist, D., Faïn, X., and Berger, C.: Gaseous elemental mercury emissions and CO(2) respiration rates in terrestrial soils under controlled aerobic and anaerobic laboratory conditions, Science of the Total Environment, 408, 1691-1700, 2010.

Obrist, D.: Mercury distribution across 14 U.S. forests. Part II: Patterns of methyl mercury concentrations and areal mass of total and methyl mercury, Environmental Science & Technology, 46, 7434, 2012.

Obrist, D., Pokharel, A. K., and Moore, C.: Vertical profile measurements of soil air suggest immobilization of gaseous elemental mercury in mineral soil, Environmental Science & Technology, 48, 2242, 2014.

Obrist, D., Agnan, Y., Jiskra, M., Olson, C. L., Colegrove, D. P., Hueber, J., Moore, C. W., Sonke, J. E., and Helmig, D.: Tundra uptake of atmospheric elemental mercury drives Arctic mercury pollution, Nature, 547, 201-+, 10.1038/nature22997, 2017.

Obrist, D., Kirk, J. L., Zhang, L., Sunderland, E. M., Jiskra, M., and Selin, N. E.: A review of global environmental mercury processes in response to human and natural perturbations: Changes of emissions, climate, and land use, Ambio, 47, 116-140, 10.1007/s13280-017-1004-9, 2018.

Outridge, P. M., Mason, R. P., Wang, F., Guerrero, S., and Heimburger-Boavida, L. E.: Updated global and oceanic mercury budgets for the united nations global mercury assessment 2018, Environmental Science & Technology, 52, 11466-11477, 10.1021/acs.est.8b01246, 2018.

Pannu, R., Siciliano, S. D., and O'Driscoll, N. J.: Quantifying the effects of soil temperature, moisture and sterilization on elemental mercury formation in boreal soils, Environmental pollution, 193, 138, 2014.

Park, S. Y., Holsen, T. M., Kim, P. R., and Han, Y. J.: Laboratory investigation of factors affecting mercury emissions from soils, Environmental Earth Sciences, 72, 2711-2721, 2014.

Peleg, M., Tas, E., Matveev, V., Obrist, D., Moore, C. W., Gabay, M., and Luria, M.: Observational evidence for involvement of nitrate radicals in nighttime oxidation of mercury, Environmental Science & Technology, 49, 14008, 2015.

© Author(s) 2019. CC BY 4.0 License.

639 Prajapati, P., and Jacinthe, P. A.: Methane oxidation kinetics and diffusivity in soils under conventional
640 tillage and long-term no-till, Geoderma, s 230–231, 161-170, 2014.
641 Renner, R.: Newly deposited mercury may be more bioavailable, Environmental Science & Technology,
642 36, 226A-227A, 10.1021/es0223224, 2002.
643 Risch, M. R., DeWild, J. F., Gay, D. A., Zhang, L., Boyer, E. W., and Krabbenhoft, D. P.: Atmospheric
644 mercury deposition to forests in the eastern USA, Environmental pollution, 228, 8-18,
645 10.1016/j.envpol.2017.05.004, 2017.
646 Ryzhakova, N. K.: A new method for estimating the coefficients of diffusion andemanation of radon in
647 the soil, Journal of Environmental Radioactivity, 135, 63-66, 2014.
648 Schlüter, K.: Review: evaporation of mercury from soils. An integration and synthesis of current
649 knowledge, Environmental Geology, 39, 249-271, 2000.
650 Schwesig, D., and Matzner, E.: Dynamics of mercury and methylmercury in forest floor and runoff of a
651 forested watershed in central Europe, Biogeochemistry, 53, 181-200, 2001.
652 Sigler, J. M., and Lee, X.: Gaseous mercury in background forest soil in the northeastern United States,
653 Journal of Geophysical Research Biogeosciences, 111, G02007, 10.1029/2005JG000106, 2006.
654 Song, S., Angot, H., Selin, N. E., Gallee, H., Sprovieri, F., Pirrone, N., Helmig, D., Savarino, J., Magand,
655 O., and Dommergue, A.: Understanding mercury oxidation and air-snow exchange on the East
656 Antarctic Plateau: a modeling study, Atmospheric Chemistry and Physics, 18, 15825-15840,
657 10.5194/acp-18-15825-2018, 2018.
658 Sørbotten, L. E.: Hill slope unsaturated flowpaths and soil moisture variability in a forested catchment
659 in Southwest China, MD, Department of Plant and Environmental Sciences, University of Life
660 Sciences, 2011.
661 Teixeira, D. C., Lacerda, L. D., and Silva-Filho, E. V.: Foliar mercury content from tropical trees and its
662 correlation with physiological parameters in situ, Environmental pollution, 242, 1050-1057,
663 10.1016/j.envpol.2018.07.120, 2018.
664 Wang, Q., Luo, Y., Du, B., Ye, Z., and Duan, L.: Influencing factors of mercury emission flux from forest
665 soil at tieshanping,chongqing, Environmental Science, 35, 1922-1927, 2014.
666 Wang, S., Feng, X., Qiu, G., Fu, X., and Wei, Z.: Characteristics of mercury exchange flux between soil
667 and air in the heavily air-polluted area, eastern Guizhou, China, Atmospheric Environment, 41,
668 5584-5594, 2007.
669 Wang, X., Lin, C.-J., Feng, X., Yuan, W., Fu, X., Zhang, H., Wu, Q., and Wang, S.: Assessment of regional
670 mercury deposition and emission outflow in mainland China, Journal of Geophysical Research-
671 Atmospheres, 123, 9868-9890, 10.1029/2018jd028350, 2018.
672 Wang, Y.: Characteristics of stand structure and hydrological function of damaged Masson pine forests
673 in the acid rain region of Chongqing, MD, Chinese Academy of Forestry, 2012.
674 Wang, Z., Zhang, X., Xiao, J., Zhijia, C., and Yu, P.: Mercury fluxes and pools in three subtropical
675 forested catchments, southwest China, Environmental pollution, 157, 801-808,
676 10.1016/j.envpol.2008.11.018, 2009.
677 Xin, M., and Gustin, M. S.: Gaseous elemental mercury exchange with low mercury containing soils:
678 Investigation of controlling factors, Applied Geochemistry, 22, 1451-1466, 2007.
679 Zhang, H., Lindberg, S. E., Marsik, F. J., and Keeler, G. J.: Mercury air/surface exchange kinetics of
680 background soils of the tahquamenon river watershed in the Michigan Upper Peninsula, Water Air
681 & Soil Pollution, 126, 151-169, 2001.
682 Zhang, H., Lindberg, S. E., Barnett, M. O., Vette, A. F., and Gustin, M. S.: Dynamic flux chamber

© Author(s) 2019. CC BY 4.0 License.

measurement of gaseous mercury emission fluxes over soils. Part 1: simulation of gaseous mercury emissions from soils using a two-resistance exchange interface model, Atmospheric Environment, 36, 835-846, 2002.

Zhou, J., Feng, X., Liu, H., Zhang, H., Fu, X., Bao, Z., Wang, X., and Zhang, Y.: Examination of total mercury inputs by precipitation and litterfall in a remote upland forest of Southwestern China, Atmospheric Environment, 81, 364-372, 10.1016/j.atmosenv.2013.09.010, 2013.

Zhou, J., Wang, Z., Zhang, X., and Chen, J.: Distribution and elevated soil pools of mercury in an acidic subtropical forest of southwestern China, Environmental pollution, 202, 187-195, 10.1016/j.envpol.2015.03.021, 2015.

Zhou, J., Wang, Z., Sun, T., Zhang, H., and Zhang, X.: Mercury in terrestrial forested systems with highly elevated mercury deposition in southwestern China: The risk to insects and potential release from wildfires, Environmental pollution, 212, 188-196, 10.1016/j.envpol.2016.01.003, 2016.

Zhou, J., Wang, Z., Zhang, X., and Gao, Y.: Mercury concentrations and pools in four adjacent coniferous and deciduous upland forests in Beijing, China, Journal of Geophysical Research Biogeosciences, 122, 1260-1274, 2017a.

Zhou, J., Wang, Z., Zhang, X., and Sun, T.: Investigation of factors affecting mercury emission from subtropical forest soil: A field controlled study in southwestern China, Journal of Geochemical Exploration, 176, 128-135, 10.1016/j.gexplo.2015.10.007, 2017b.

Zhou, J., Wang, Z., and Zhang, X.: Deposition and fate of mercury in litterfall, litter, and soil in coniferous and broad-leaved forests, Journal of Geophysical Research-Biogeosciences, 123, 2590-2603, 10.1029/2018jg004415, 2018.

Zhu, W., Lin, C. J., Wang, X., Sommar, J., Fu, X., and Feng, X.: Global observations and modeling of atmosphere-surface exchange of elemental mercury: a critical review, Atmospheric Chemistry & Physics, 16, 4451-4480, 2016.

Atmos. Chem. Phys. Discuss., https://doi.org/10.5194/acp-2019-161
Manuscript under review for journal Atmos. Chem. Phys.
Discussion started: 18 March 2019
© Author(s) 2019. CC BY 4.0 License.

709 **Table 1.** Locations and detailed measurements of soil-air flux, soil pore TGM concentrations and environmental parameters at five plots in the subtropical forest.

Plots	Locations	Soil surface TGM (ng m^{-3})	Soil pore TGM (ng m^{-3})					Flux	Soil Hg concentration (ng g^{-1})	Soil moisture (%)	Soil temperature (°C)	Solar radiation (W m^{-2})
			3 cm	6 cm	10 cm	20 cm	50 cm					
Plot A	Top-slope of coniferous forest	3.6±1.3	8.4±7.9	9.8±8.7	13.0±12.2	12.5±10.2	13.0±9.8	2.8 ± 3.9	219±15	0.3±0.1	16.8±7.6	39.9±27.5
Plot B	Middle-slope of the coniferous forest	3.8±1.3	10.0±6.2	11.9±6.1	15.1±9.8	12.7±7.9	10.4±7.4	3.5 ± 4.2	263±22	0.4±0.1	16.9±7.7	40.2±27.5
Plot C	Wetland	3.7±1.4						-0.80 ± 5.1	96±43	0.3±0.1	16.7±7.5	20.5±27.9
Plot D	Broad-leaved forest	3.3±1.4	8.0±4.8	7.1±4.3	6.2±3.4	6.2±2.0	5.8±2.8	0.18 ± 4.3	156±17	0.3±0.1	16.9±7.6	20.3±27.9
Plot E	Open field (bare soil)	4.1±1.7	12.9±11.0	18.5±16.9	14.1±9.2	17.0±9.7	16.6±10.1	24 ± 33	159±18	0.3±0.1	18.3±8.5	98.0±138.4

710
711

© Author(s) 2019. CC BY 4.0 License.

712

713 **Figure Captions:**

714

715 **Fig. 1.** Location of the five sampling plots and the estimation of Hg mass-balance at the TFP
716 subtropical forest (blue square: flux sampling site; spiral line: Soil pore TGM sampling site).
717 Litterfall Hg deposition was from Zhou et al. (2018); throughfall Hg deposition was from Luo
718 et al. (2015); surface runoff (SR) Hg flux was from Zhou et al. (2015); wet Hg deposition was
719 from Wang et al. (2009); soil Hg pools were from Zhou et al. (2016); UR means underground
720 runoff.

721 **Fig. 2.** Mean and standard deviation of soil-air TGM fluxes at the five plots for the four seasons and
722 annual values during the study. Plots A, B and C was located in the coniferous forest, plot D
723 was in the broad-leaved forest, and plot E was in the open field. The data numbers of flux in
724 spring, summer, autumn and winter are 62, 92, 66 and 43.

725 **Fig. 3.** The daily variation trends of Hg fluxes with meteorological parameters in spring (a), summer
726 (b), autumn (c) and winter (d) at the coniferous forest.

727 **Fig. 4.** Comparison between model-predicted and DFC-measured fluxes of Hg for the five plots.
728 DFC-measured flux is a daily flux averaging daytime and night values.

729 **Fig. 5.** Contour plots of soil pore TGM concentrations which in order are plots A, B, D and E. plots
730 were created based on daytime and night pore TGM measurements combining soil surface (3
731 cm) and 5 soil layers (3 cm, 6cm, 10cm, 20cm and 50cm).

732 **Fig. 6.** Scatter plots and linear regressions between soil-air fluxes and the gradient of TGM
733 concentration divided the distance between soil pore TGM at 3 cm (*Cs*) and the atmosphere
734 above the plot (*Ca*) based on the two-resistance exchange interface model. The relationships
735 were based on night flux and soil TGM measurements, and were significant at the respective
736 plots ($p<0.05$).

737

Atmos. Chem. Phys. Discuss., https://doi.org/10.5194/acp-2019-161
Manuscript under review for journal Atmos. Chem. Phys.
Discussion started: 18 March 2019
© Author(s) 2019. CC BY 4.0 License.

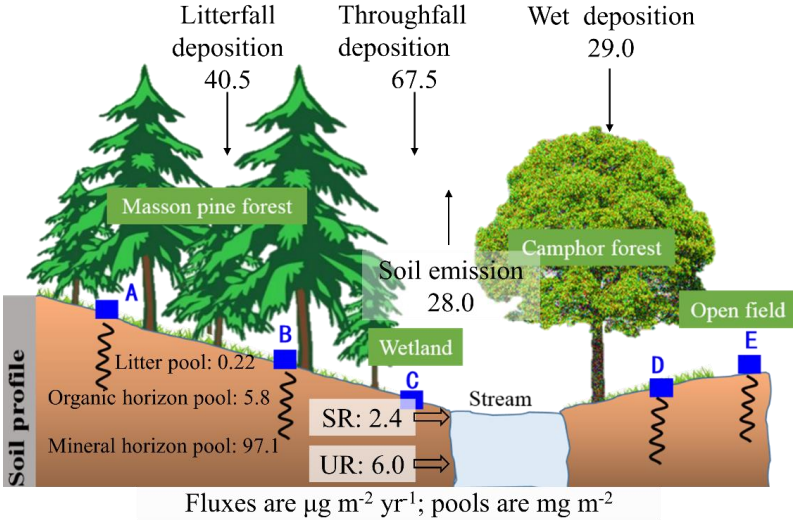

738
739 **Fig. 1.** Location of the five sampling plots and the estimation of Hg mass-balance at the TFP
740 subtropical forest (blue square: flux sampling site; spiral line: Soil pore TGM sampling site).
741 Litterfall Hg deposition was from Zhou et al. (2018); throughfall Hg deposition was from Luo et al.
742 (2015); surface runoff (SR) Hg flux was from Zhou et al. (2015); wet Hg deposition was from Wang
743 et al. (2009); soil Hg pools were from Zhou et al. (2016); UR means underground runoff.
744

Atmos. Chem. Phys. Discuss., https://doi.org/10.5194/acp-2019-161
Manuscript under review for journal Atmos. Chem. Phys.
Discussion started: 18 March 2019
© Author(s) 2019. CC BY 4.0 License.

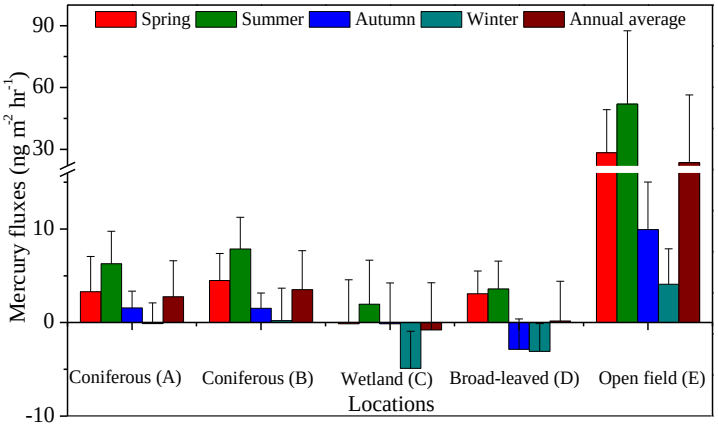

745

746 **Fig. 2.** Mean and standard deviation of soil-air TGM fluxes at the five plots for the four seasons and
747 annual values during the study. Plots A, B and C was located in the coniferous forest, plot D was in
748 the broad-leaved forest, and plot E was in the open field. The data numbers of flux in spring, summer,
749 autumn and winter are 62, 92, 66 and 43.
750

Atmos. Chem. Phys. Discuss., https://doi.org/10.5194/acp-2019-161
Manuscript under review for journal Atmos. Chem. Phys.
Discussion started: 18 March 2019
© Author(s) 2019. CC BY 4.0 License.

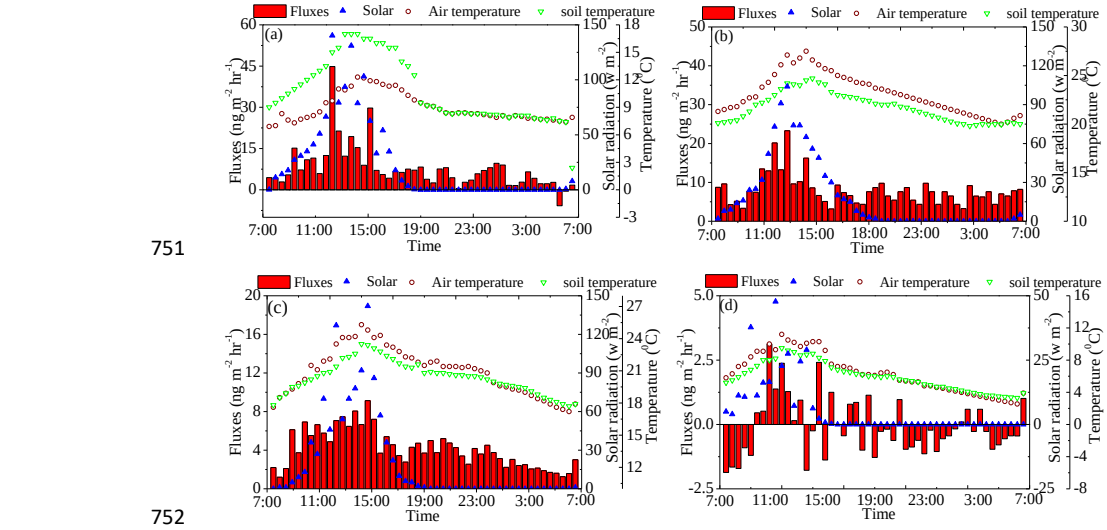

Fig. 3. The daily variation trends of Hg fluxes with meteorological parameters in spring (a), summer (b), autumn (c) and winter (d) at the coniferous forest.

Atmos. Chem. Phys. Discuss., https://doi.org/10.5194/acp-2019-161
Manuscript under review for journal Atmos. Chem. Phys.
Discussion started: 18 March 2019
© Author(s) 2019. CC BY 4.0 License.

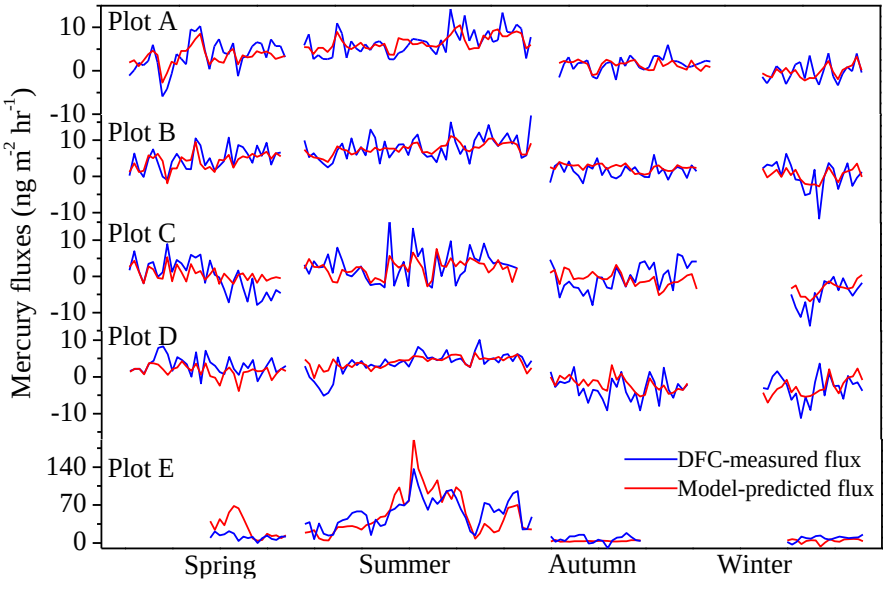

Fig. 4. Comparison between model-predicted and DFC-measured fluxes of Hg for the five plots. DFC-measured flux is a daily flux averaging daytime and night values.

Atmos. Chem. Phys. Discuss., https://doi.org/10.5194/acp-2019-161
Manuscript under review for journal Atmos. Chem. Phys.
Discussion started: 18 March 2019
© Author(s) 2019. CC BY 4.0 License.

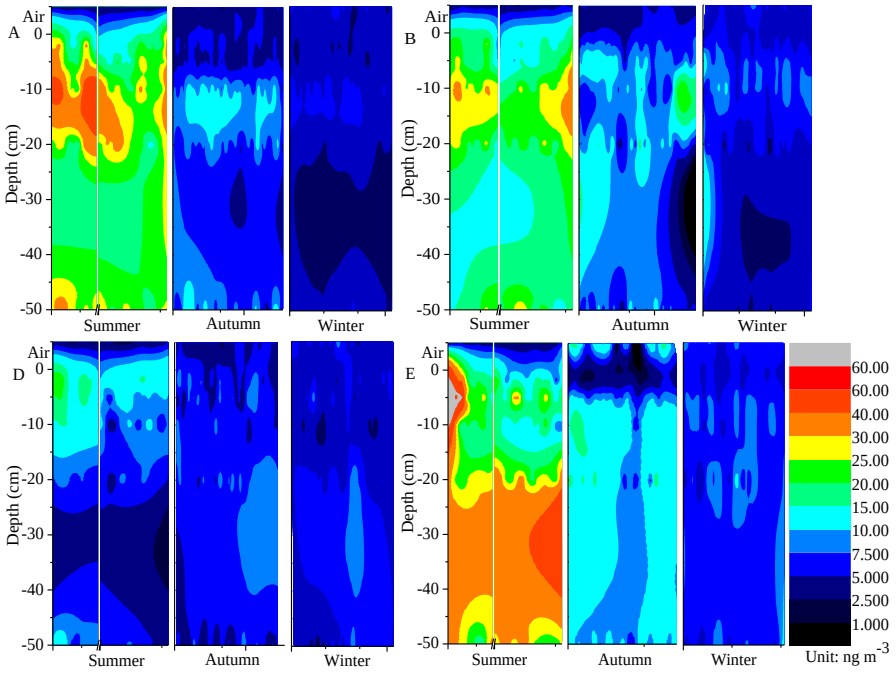

Fig. 5. Contour plots of soil pore TGM concentrations which in order are plots A, B, D and E. plots were created based on daytime and night pore TGM measurements combining soil surface (3 cm) and 5 soil layers (3 cm, 6cm, 10cm, 20cm and 50cm).

Atmos. Chem. Phys. Discuss., https://doi.org/10.5194/acp-2019-161
Manuscript under review for journal Atmos. Chem. Phys.
Discussion started: 18 March 2019
© Author(s) 2019. CC BY 4.0 License.

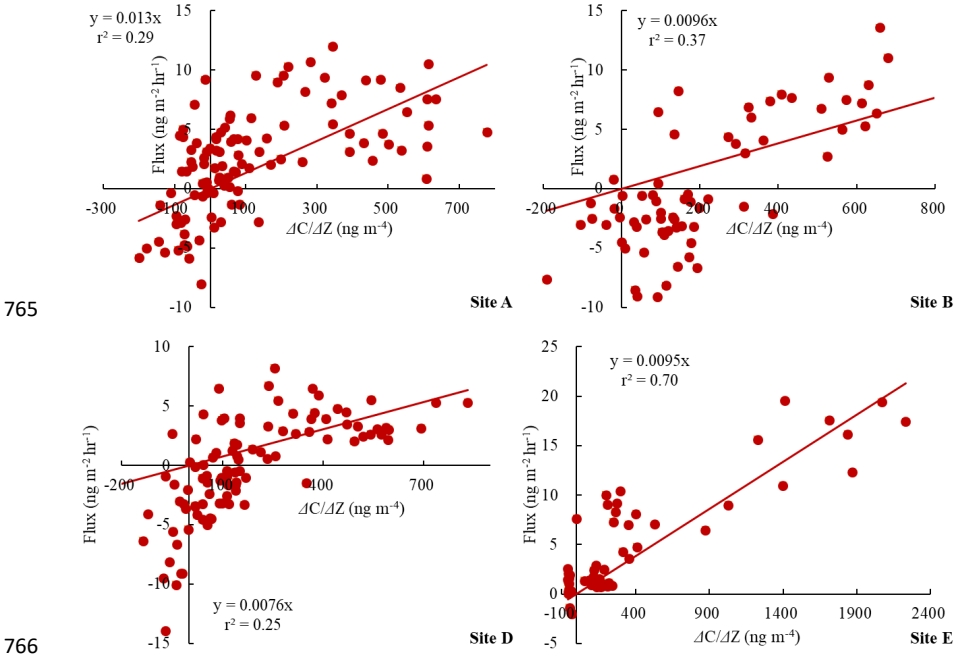

Fig. 6. Scatter plots and linear regressions between soil-air fluxes and the gradient of TGM concentration divided the distance between soil pore TGM at 3 cm (*Cs*) and the atmosphere above the plot (*Ca*) based on the two-resistance exchange interface model. The relationships were based on night flux and soil TGM measurements, and were significant at the respective plots ($p<0.05$).